Letter

Imaging Andreev Reflection in Graphene

Sagar Bhandari, Gil-Ho Lee, Kenji Watanabe, Takashi Taniguchi, Philip Kim, and Robert M. Westervelt*

Read Online

ACCESS | 📊 Metrics & More | 📰 Article Recommendations

ABSTRACT: Coherent charge transport along ballistic paths can be introduced into graphene by Andreev reflection, for which an electron reflects from a superconducting contact as a hole, while a Cooper pair is transmitted. We use liquid-helium cooled scanning gate microscopy (SGM) to image Andreev reflection in graphene in the magnetic focusing regime, where carriers move along cyclotron orbits between contacts. Images of flow are obtained by deflecting carrier paths and displaying the resulting change in conductance. When electrons enter the superconductor, Andreev-reflected holes leave for the collecting contact. To test the results, we destroy Andreev reflection with a large current and by heating above the critical temperature. In both cases, the reflected carriers change from holes to electrons.

KEYWORDS: graphene, Andreev reflection, ballistic transport, scanning gate microscope
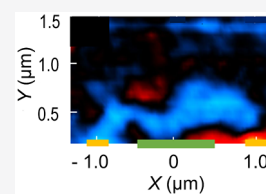
G raphene is a remarkable material that allows electrons to travel across a sample without collisions.[1,2] Coherent charge transport over ballistic trajectories can be introduced into graphene from superconductors by using Andreev scattering[3−6] or Josephson coupling.[7−14] For Andreev reflection, an electron reflects from a superconducting contact as a hole, while a Cooper pair is transmitted. Graphene/superconductor hybrid devices show coherent phenomena including crossed Andreev conversion[7] and edge states in graphene Josephson junctions.[8] Here, we employ liquid-helium cooled scanning gate microscopy (SGM)[15−26] to image Andreev reflection in graphene from a superconducting contact in the magnetic focusing regime. The SGM images the ballistic paths of electrons or holes by deflecting their trajectories and displaying the resulting change in conductance.[19,21] The images show cyclotron orbits of electrons entering the superconductor and Andreev-reflected holes leaving for the collecting contact. To confirm the results, we destroy Andreev reflection by applying a large current and by heating the sample above the critical temperature. For both cases, the collected carriers change from holes to electrons.

Andreev reflection[3−5] is the process that links carriers in graphene with a superconducting contact; Figure 1(a) shows how this occurs. An electron enters the superconducting contact at an energy $E_F + eV_{bs}$, where eV_{bs} is less than the superconducting energy gap Δ. A hole is reflected back into the graphene with energy $E_F − eV_{bs}$, as well as a Cooper pair that passes into the superconductor. Energy, momentum, and charge are conserved. These processes are indicated on the graphene band structure E vs k shown on the right—note that the electron and Andreev-reflected hole are both near E_F in the conduction band.

Andreev reflection provides a microscopic description of the superconducting proximity effect and explains how non-superconducting charge carriers gain the superconducting correlation. This process is essential for superconducting hybrid systems, including superconducting quantum circuits, Josephson junctions, and topological superconductivity. Spatial imaging of Andreev reflection in a ballistic conductor shows how the superconducting proximity effect can be used to create coherent ballistic paths for charge carriers in a hybrid system.

Here, we use magnetic focusing to track the motion of electrons and Andreev-reflected holes through a graphene device with transparent niobium (Nb) superconducting contacts, as illustrated in Figure 1(b) and (c). A perpendicular magnetic field B bends carrier motion into circular cyclotron orbits with diameter $d_c = (n/\pi)^{1/2}h/eB$, where n is the carrier density and e is the elementary charge. A magnetic focusing peak occurs when carriers leaving the first contact are rejoined at a second contact spaced a distance d_c away. Figure 1(b) illustrates the reflection of electrons that occurs from a normal center contact in the magnetic focusing regime, i.e. an electron impinging on the contact is reflected as an electron and travels along a cyclotron orbit to the right contact. Like the incoming carrier, the reflected electron has a negative charge $−e$, and a positive cyclotron mass m_e^*. Figure 1(c) shows how Andreev reflection occurs for a superconducting center contact when the electron and hole are both in the conduction band. In this case, an electron entering the superconducting center contact is reflected as a hole which has a positive charge $+e$, and a negative cyclotron mass $−m_e^*$. The hole rotates in a clockwise direction along a cyclotron orbit, in the same direction as an electron, because the charge and cyclotron mass of the hole
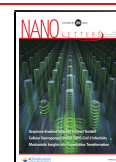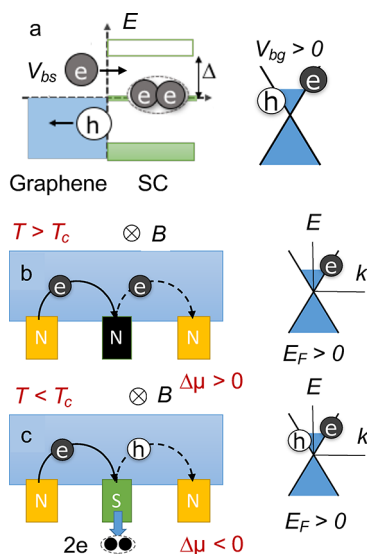
Figure 1. Andreev-reflection in a graphene device with superconducting contacts. In the following, E_F is the Fermi energy, Δ is the superconducting energy gap, and e is the electronic charge. (a) For Andreev reflection, an electron with energy $E_F + eV_{bs}$ entering a superconducting contact with $eV_{bs} < \Delta$ generates a hole with energy $E_F - eV_{bs}$ that is reflected back into the graphene and a Cooper pair that passes into the superconductor. The dispersion relation of E vs k of graphene is shown on the right. (b) Illustration of magnetic focusing of electron orbits for a graphene sample with normal contacts in a perpendicular magnetic field B when the cyclotron diameter matches the contact spacing. (c) For a superconducting center contact, Andreev reflection converts an incoming electron into an outgoing hole with positive charge that flows to the right contact and a Cooper pair that passes into the superconductor.

both have a reversed sign compared with an electron, and the two factors cancel. An immediate indicator for Andreev reflection is that the voltage signal on the right contact changes sign, because holes are arriving instead of electrons, as shown below.

Figure 2 shows a scanning electron micrograph of the graphene device, which was fabricated from a hexagonal boron nitride (hBN) encapsulated monolayer graphene sheet with a 35 nm thick hBN layer on top and a 45 nm hBN layer on bottom, which was placed on an Si substrate with a 300 nm thick SiO_2 layer that acts as a back gate. The encapsulated sheet was shaped into a Hall bar with five Nb superconducting contacts S1, S2, S3, S4, and S5, with critical temperature T_c = 8.0 K. The sample was mounted inside the cooled scanning gate microscope in an inner chamber filled with He-4 gas at 3 Torr surrounded by liquid He at 4.2 K. A perpendicular magnetic field B was applied using a superconducting solenoid. The semicircles in Figure 2(a) illustrate the expected cyclotron orbits of electrons, shown in red, and Andreev-reflected holes, shown in blue. To record the ballistic flow of carriers, a current I is passed from S2 to contacts S1 and S3, which are grounded. Ballistic carriers flow to the opposite side of the sample, where they are collected by contacts S4 and S5, which are floating. The voltage difference $V_m = IR_m$ between contacts S4 and S5 is proportional to the transmission T_m from S2 to S4. The flow of electrons into contact S4 increases its electron density and chemical potential, creating a equal and opposite flow that zeroes the total current. The voltage $V_m \sim \Delta\mu$ is positive, given the sign of I. On the other hand, a flow of Andreev-reflected holes into S4 decreases the electron density and chemical
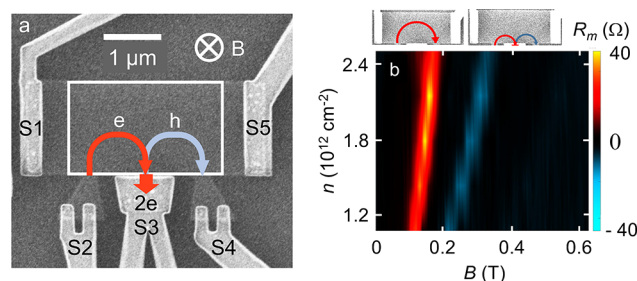

Figure 2. Magnetic focusing of Andreev reflection in graphene. (a) Scanning electron micrograph of the hBN-encapsulated graphene device on an Si/SiO_2 substrate with superconducting contacts S1, S2, S3, S4, and S5. The red and blue semicircles illustrate the cyclotron orbits of an electron and an Andreev-reflected hole in a perpendicular magnetic field B. The current I enters the device from S2 while S1 and S3 are grounded, and the voltage V_m between S4 and S5 is measured. (b) Measured transresistance $R_m = V_m / I$ is displayed vs B and electron density n at 4.2 K. The first magnetic focusing peak (red) between the outer contacts S2 and S4 occurs when the electron cyclotron diameter matches their separation. A second magnetic focusing peak (blue) of opposite sign occurs when electrons from S2 travel along a cyclotron orbit to S3 and are Andreev-reflected as holes that follow an orbit to S4.

potential and creates a signal $V_m \sim -\Delta\mu$ that is negative. The change of sign in the detected signal allows us to determine whether the carriers collected by contact S4 are electrons or Andreev-reflected holes, as demonstrated below.

To determine the magnetic field B and electron density n at which magnetic focusing occurs, the measured transresistance R_m is displayed versus B and n at 4.2 K in Figure 2(b). The first "peak", shown in red ($R_m > 0$), corresponds to magnetic focusing of electrons between the two outer contacts S2 and S4, as illustrated in the inset to Figure 2(b). At larger B, a second "peak", shown in the color blue ($R_m < 0$), corresponds to magnetic focusing of Andreev-reflected holes between the center and right contacts, S3 and S4, also illustrated in Figure 2(b). The sign of the signal R_m is reversed, indicating that the carriers collected by S4 are now holes instead of electrons.

Images of the flow of electrons and Andreev-reflected holes through the graphene device recorded by our cooled scanning probe microscope in the magnetic focusing regime are shown in Figures 3 and 4 below. The imaging technique is described in detail for our previous imaging experiments on graphene.[25,26] A charged tip is scanned at a constant height above the graphene device. The tip creates an image charge in the two-dimensional electron gas (2DEG) by pushing electrons away. An image of ballistic flow between two contacts is obtained by displaying the measured change ΔR_m as the tip is raster scanned across the sample, deflecting ballistic electrons away from their original trajectories and changing the transmission by ΔT_m.[25,26]

In our earlier imaging work on graphene,[25,26] we described how to simulate SGM images of carrier flow by ray-tracing carrier trajectories. The negatively charged SGM tip pushes electrons away, creating a local dip in electron density and Fermi energy E_F with a width $\sim$70 nm that is comparable to the height of the tip above the graphene layer. In equilibrium, the total chemical potential $E_F + U$ must be constant, where U is the potential energy created by the tip. The force $\vec{F} = -\vec{\nabla} U$ from the tip creates an outward current that is balanced by an inward diffusive flow of electrons to fill the dip.
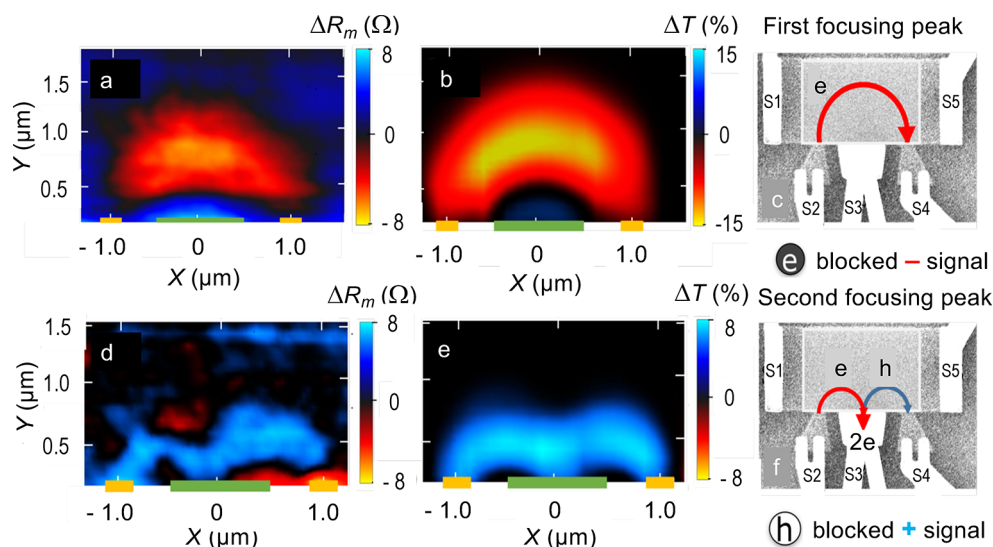
Figure 3. Images of Andreev reflection in graphene from a superconducting contact. (a) SGM image at the first magnetic focusing peak showing cyclotron orbits of electrons in red ($\Delta R_m < 0$) from contact S2 to S4, taken at $B = 0.13$ T, $n = 1.8 \times 10^{12}$ cm^{-2}, and 4.2 K. The image displays the change ΔR_m in the flow vs tip position, as the tip deflects electrons away from their original orbits. (b) Corresponding simulated image of the transmission change ΔT due to deflected orbits. (c) Electron orbit (red) from contact S2 to S4. (d) SGM image of Andreev reflection taken on the second magnetic focusing peak at $B = 0.26$ T. The image shows two cyclotron orbits, one for electrons traveling from contact S2 to S3 and one for Andreev-reflected holes traveling from contact S3 to S4. Both orbits are shown in blue ($\Delta R_m > 0$), because holes arrive at contact S4 in both cases, instead of electrons. Blocking an electron flowing from contact S2 to S3 also blocks the Andreev-reflected hole that would have traveled to contact S4. (e) Corresponding simulated image of ΔT vs tip position. (f) Electron orbit from contact S2 to S3, and the Andreev-reflected hole orbit from S3 to S4.
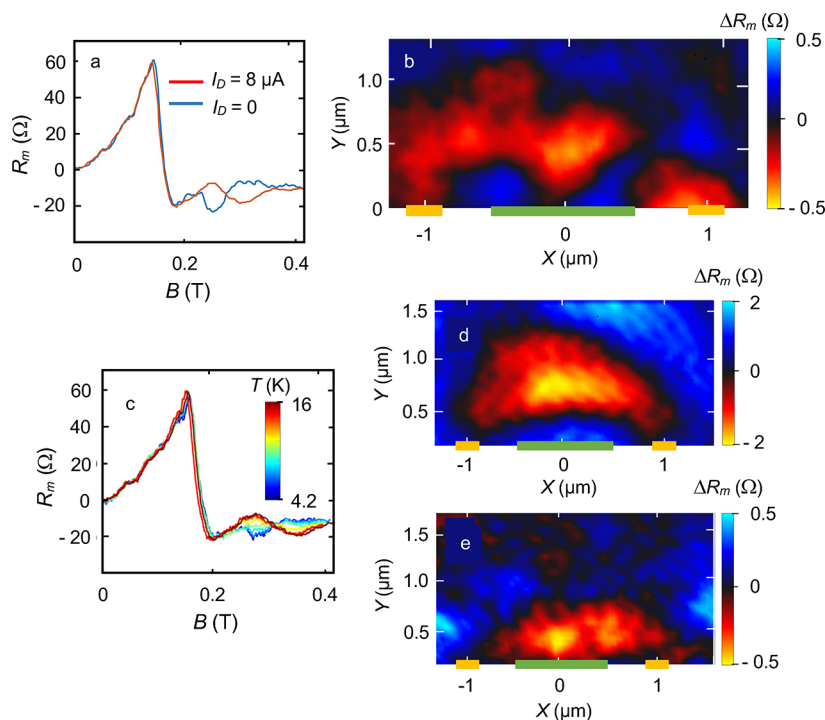

Figure 4. Destruction of Andreev reflection by a current I_{DC} and by heating above the critical temperature $T_c = 8.0$ K of the superconducting contact. (a) Plots of electron flow R_m vs B for $n = 1.8 \times 10^{12}$ cm^{-2} show the first magnetic focusing peak at $B = 0.13$ T and a feature in R_m at the second magnetic focusing field $B = 0.26$ T. For $I_{DC} = 0$, a dip (blue) occurs at $B = 0.26$ T when Andreev-reflected holes arrive at S4. For $I_{DC} = 8 \mu$A, the electron energy is too high to undergo Andreev reflection, and the dip at $B = 0.26$ T changes into a peak (red) from normally reflected electrons. (b) The corresponding SGM image is red ($\Delta R_m < 0$) for $I_{DC} = 8 \mu$A, because normally reflected electrons flow into S4 instead of Andreev-reflected holes. (c) Plots of R_m vs B for 4.2 to 16 K showing that heating changes the dip in R_m at $B = 0.26$ T into a peak due to normally reflected electrons. (d) SGM image at 16 K showing electron orbits in red ($\Delta R_m < 0$) from S2 to S4 for $B = 0.13$ T. (e) The SGM image at 16 K on the second magnetic focusing peak at $B = 0.26$ T has normally reflected electron orbits in red ($\Delta R_m < 0$) when contact S3 is normal.

The outward force $\vec{F} = -\vec{\nabla}U = \vec{\nabla}E_F$ also acts on non-equilibrium electrons passing nearby. The transmission T between contacts S2 and S4 was found by ray-tracing simulations; the trajectories of a large number of carriers that enter at random angles from S2 were calculated using the classical equation of motion, and the transmission T was found by counting the fraction that reach the collecting contact S4.[25,26]

The SGM images in Figure 3 clearly demonstrate how the transition from normal to Andreev reflection occurs for $n = 1.8 \times 10^{12}$ cm^{-2} at 4.2 K. The top three panels of Figure 3, (a), (b), and (c), show the flow of electrons along cyclotron orbits between the two outer contacts, S2 and S4, on the first magnetic focusing peak at $B = 0.13$ T in Figure 2(b). Figure 3(a) presents an SGM image of electron flow from S2 to S4; Figure 3(b) shows the corresponding simulations, which are in good agreement, and Figure 3(c) shows the path of electron orbits on a scanning electron micrograph of the device. We chose the color red to represent electrons for the SGM images in Figure 3, where the change $\Delta R_m < 0$, because electrons are deflected by the tip. We also chose the color red to represent electron flow for magnetic focusing measurements in Figure 2(b), where $R_m > 0$. On the other hand, we chose the color blue to represent Andreev-reflected holes for the SGM images in Figure 3 where the change $\Delta R_m > 0$ when holes are deflected by the tip and the color blue to represent magnetic focusing measurements in Figure 2(b), where $R_m < 0$ when holes are collected by contact S4.

The lower three panels of Figure 3, (a), (b), and (c), show Andreev reflection of holes from the superconducting center contact, taken on the second magnetic peak at $B = 0.26$ T and $n = 1.8 \times 10^{12}$ cm^{-2} in Figure 2(b). Figure 3(d) is an SGM image of electron flow along cyclotron orbits from contact S2 to the superconducting center contact S3, as well as the flow of Andreev-reflected holes along cyclotron orbits from S3 to the collecting contact S4. In Figure 3(d), the electron and hole orbits are both shown in the color blue ($\Delta R_m > 0$), because Andreev-reflected holes enter S4 in both cases; if the tip deflects an electron orbit traveling from S2 to S3, the Andreev-reflected hole traveling from S3 to S4 is also lost. Charge is conserved during Andreev reflection, because an electron entering the superconducting contact S3 leaves as a Cooper pair that flows to ground and as an Andreev-reflected hole that travels to S4. Figure 3(f) shows ray-tracing simulations of Andreev reflection, which are in good agreement, and Figure 3(g) shows the paths of the electron orbits traveling from S2 to S3 and the Andreev-reflected hole orbits traveling from S3 to S4. The use of magnetic focusing to confine carrier paths allows us to clearly distinguish Andreev-reflected holes from normally reflected electrons. Our SGM imaging technique can also be used to characterize Andreev reflection in other circumstances when a magnetic field is not present.

To verify that Andreev reflection causes the patterns of carrier flow observed in Figure 3, we destroyed the effect by adding an emitter current $I_{DC} = 8$ μA for which the emitted electron energy $eV_{bs} > \Delta$ is too large to undergo Andreev reflection. Figure 4 (a) plots the magnetic-focusing signal R_m vs B for $n = 1.8 \times 10^{12}$ cm^{-2} at 4.2 K, similar to the data shown in Figure 2(b). As the magnetic field is increased from $B = 0$ to 0.13 T, the signal R_m forms the first magnetic focusing peak for electron flow along cyclotron orbits between the two outer contacts S2 and S4. As B continues to increase, R_m abruptly

drops to a minimum at $B = 0.19$ T when the diameter of the cyclotron orbit drops below the spacing between S2 and S4, an effect shown by the simulated orbits in Figure 3(b). For $I_{DC} = 0$, the second magnetic focusing feature at $B = 0.26$ T occurs as a dip in R_m, as shown in Figure 4(a), because Andreev-reflected holes enter the collecting contact S4, after traveling from the superconducting center contact S3. When a large current $I_{DC} = 8$ μA is added, Andreev reflection is destroyed, and the dip in R_m for the second magnetic focusing feature at $B = 0.26$ T changes to a local maximum, as shown in Figure 4(a), because normally reflected electrons from contact S3 now enter the collecting contact S4 instead of holes. Please note that the baseline and magnetic focusing peak shapes in Figure 4(a) differ slightly from those in Figure 2(b), due to a drift in the electrical properties over the duration of the measurements.

The destruction of Andreev reflection by a large current $I_{DC} = 8$ μA is visualized by the SGM image of normally reflected electrons shown in red ($\Delta R_m < 0$) in Figure 4(b), taken on the second magnetic focusing peak for $B = 0.26$ T and $n = 1.8 \times 10^{12}$ cm^{-2}. When the current is off ($I_{DC} = 0$), the SGM image in Figure 3(d) shows Andreev reflection of holes from the superconducting center contact S3 under the same conditions. The transformation of Andreev-reflected holes to normally reflected electrons when a large current $I_{DC} = 8$ μA is applied confirms that Andreev reflection has been destroyed.

We conducted an additional verification that Andreev reflection was observed by heating the device above the critical temperature $T_c = 8.0$ K of the superconducting contact S3. Figure 4(c) plots the magnetic focusing signal R_m vs B at temperatures ranging from 4.2 K (red) to 16 K (blue). As noted above, the dip in R_m at $B = 0.26$ T is a caused by Andreev reflection. As the sample is warmed above 8 K, the dip for Andreev-reflected holes changes sign to become the second magnetic focusing peak for normally reflected electrons. Corresponding SGM images at 16 K in Figure 4(d) and (e) support these identifications. Figure 4(d) shows the flow of electrons in red ($\Delta R_m < 0$) between contacts S2 and S4 on the first magnetic focusing peak at $B = 0.13$ T, which is similar to Figure 3(a) as expected. The effect of raising the temperature above T_c is seen in the SGM image in Figure 4(e), which shows normally reflected electrons in red ($\Delta R_m < 0$) on the second magnetic focusing peak. Below T_c, the SGM image at $B = 0.26$ T in Figure 3(d) shows Andreev reflected holes in blue ($\Delta R_m > 0$) instead. These SGM images confirm that heating above the superconducting critical temperature T_c destroyed Andreev reflection, as expected, and that normally reflected electrons enter the collecting contact S4 instead of Andreev reflected holes.

◼ AUTHOR INFORMATION

Corresponding Author

Robert M. Westervelt − *School of Engineering and Applied Sciences and Department of Physics, Harvard University, Cambridge, Massachusetts 02138, United States;* ⬥ orcid.org/0000-0001-9836-3923; Email: westervelt@seas.harvard.edu

Authors

Sagar Bhandari − *School of Engineering and Applied Sciences, Harvard University, Cambridge, Massachusetts 02138, United States; Department of Physics and Engineering, Slippery Rock University, Slippery Rock, Pennsylvania 16057, United States*

Gil-Ho Lee − *Department of Physics, Harvard University, Cambridge, Massachusetts 02138, United States; Department of Physics, Pohang University of Science and Technology, Pohang 790-784, Republic of Korea*

Kenji Watanabe − *National Institute for Materials Science, Tsukuba 305-0044, Japan;* orcid.org/0000-0003-3701-8119

Takashi Taniguchi − *National Institute for Materials Science, Tsukuba 305-0044, Japan;* orcid.org/0000-0002-1467-3105

Philip Kim − *School of Engineering and Applied Sciences and Department of Physics, Harvard University, Cambridge, Massachusetts 02138, United States;* orcid.org/0000-0002-8255-0086

Complete contact information is available at:
https://pubs.acs.org/10.1021/acs.nanolett.0c00903

Notes
The authors declare no competing financial interest.

◼ REFERENCES

(1) Geim, A.; Novoselov, K. The rise of graphene. *Nat. Mater.* **2007**, *6*, 183−191.

(2) Dean, C. R.; Young, A. F.; Meric, I.; Lee, C.; Wang, L.; Sorgenfrei, S.; Watanabe, K.; Taniguchi, T.; Kim, P.; Shepard, K. L.; Hone, J. Boron nitride substrates for high-quality graphene electronics. *Nat. Nanotechnol.* **2010**, *5*, 722−726.

(3) Andreev, A. F. The Thermal Conductivity of the Intermediate State in Superconductors. *Sov. Phys. JETP* **1964**, *19*, 1228.

(4) Beenakker, C. W. J. Specular Andreev reflection in graphene. *Phys. Rev. Lett.* **2006**, *97*, 067007.

(5) Beenakker, C. W. J. Colloquium: Andreev reflection and Klein tunneling in graphene. *Rev. Mod. Phys.* **2008**, *80*, 1337−1354.

(6) Efetov, D. K.; Wang, L.; Handschin, C.; Efetov, K. B.; Shuang, J.; Cava, R.; Taniguchi, T.; Watanabe, K.; Hone, J.; Dean, C. R.; Kim, P. Specular interband Andreev reflections at van der Waals interfaces between graphene and NbSe$_2$. *Nat. Phys.* **2016**, *12*, 328−332.

(7) Lee, G.-H.; Huang, K.-F.; Efetov, D. K.; Wei, D. S.; Hart, S.; Taniguchi, T.; Watanabe, K.; Yacoby, A.; Kim, P. Inducing superconducting correlation in quantum Hall edge states. *Nat. Phys.* **2017**, *13*, 693−698.

(8) Allen, M. T.; Shtanko, S.; Fulga, I. C.; Akhmerov, A. R.; Watanabe, K.; Taniguchi, T.; Jarillo-Herrero, P.; Levitov, L. S.; Yacoby, A. Spatially resolved edge currents and guided wave electronic states in graphene. *Nat. Phys.* **2016**, *12*, 128−133.

(9) Heersche, H. B.; Jarillo-Herrero, P.; Oostinga, J. B.; Vandersypen, L. M. K.; Morpurgo, A. F. Bipolar supercurrent in graphene. *Nature* **2007**, *446*, 56−59.

(10) Mizuno, N.; Nielsen, B.; Du, X. Ballistic-like supercurrent in suspended graphene Josephson weak links. *Nat. Commun.* **2013**, *4*, 2716.

(11) Lee, G.-H.; Kim, S.; Jhi, S.-H.; Lee, H. J. Ultimately short ballistic vertical graphene Josephson junctions. *Nat. Commun.* **2015**, *6*, 6181.

(12) Calado, V. E.; Goswami, S.; Nanda, G.; Diez, M.; Akhmerov, A. R.; Watanabe, K.; Taniguchi, T.; Klapwijk, T. M.; Vandersypen, L. M. K. Ballistic Josephson junctions in edge-contacted graphene. *Nat. Nanotechnol.* **2015**, *10*, 761−764.

(13) Ben Shalom, M.; Zhu, M. J.; Fal'ko, V. I.; Mishchenko, A.; Kretinin, A. V.; Novoselov, K. S.; Woods, C. R.; Watanabe, K.; Taniguchi, T.; Geim, A. K.; Prance, J. R. Quantum oscillations of the critical current and high-field superconducting proximity in ballistic graphene. *Nat. Phys.* **2016**, *12*, 318−322.

(14) Amet, F.; Ke, C. T.; Borzenets, I. V.; Wang, J.; Watanabe, K.; Taniguchi, T.; Deacon, R. S.; Yamamoto, M.; Bomze, Y.; Tarucha, S.; Finkelstein, G. Supercurrent in the quantum Hall regime. *Science* **2016**, *352*, 966−969.

(15) Tessmer, S. H.; Glicofridis, P. I.; Ashoori, R. C.; Levitov, L. S.; Melloch, M. R. Subsurface charge accumulation imaging of a quantum Hall liquid. *Nature* **1998**, *392*, 51−54.

(16) Yacoby, A.; Hess, H. F.; Fulton, T. A.; Pfeiffer, L. N.; West, K. W. Electrical imaging of the quantum Hall state. *Solid State Commun.* **1999**, *111*, 1−13.

(17) McCormick, K. L.; Woodside, M. T.; Huang, M.; Wu, M.; McEuen, P. L.; Duruoz, C.; Harris, J. S., Jr. Scanned potential microscopy of edge and bulk currents in the quantum Hall regime. *Phys. Rev. B: Condens. Matter Mater. Phys.* **1999**, *59*, 4654−4657.

(18) Crook, R.; Smith, C. G.; Simmons, M. Y.; Ritchie, D. A. Imaging cyclotron orbits and scattering sites in a high-mobility two-dimensional electron gas. *Phys. Rev. B: Condens. Matter Mater. Phys.* **2000**, *62*, 5174−5178.

(19) Topinka, M. A.; Leroy, B. J.; Shaw, S. E. J.; Fleischmann, R.; Heller, E. J.; Westervelt, R. M.; Maranowski, K. D.; Gossard, A. C. Imaging Coherent Electron Flow from a Quantum Point Contact. *Science* **2000**, *289*, 2323−2326.

(20) Pioda, A.; Kičin, S.; Ihn, T.; Sigrist, M.; Fuhrer, A.; Ensslin, K.; Weichselbaum, A.; Ulloa, S. E.; Reinwald, M.; Wegscheider, W. Spatially Resolved Manipulation of Single Electrons in Quantum Dots Using a Scanned Probe. *Phys. Rev. Lett.* **2004**, *93*, 216801.

(21) LeRoy, B. J.; Bleszynski, A. C.; Aidala, K. E.; Westervelt, R. M.; Kalben, A.; Heller, E. J.; Shaw, S. E. J.; Maranowski, K. D.; Gossard, A. C. Imaging Electron Interferometer. *Phys. Rev. Lett.* **2005**, *94*, 126801.

(22) Steele, G. A.; Ashoori, R. C.; Pfeiffer, L. N.; West, K. W. Imaging transport resonances in the quantum Hall effect. *Phys. Rev. Lett.* **2005**, *95*, 136804.

(23) Jura, M. P.; Topinka, M. A.; Urban, L.; Yazdani, A.; Shtrikman, H.; Pfeiffer, L. N.; West, K. W.; Goldhaber-Gordon, D. Unexpected features of branched flow through high-mobility two-dimensional electron gases. *Nat. Phys.* **2007**, *3*, 841.

(24) Aidala, K. E.; Parrott, R. E.; Kramer, T.; Heller, E. J.; Westervelt, R. M.; Hanson, M. P.; Gossard, A. C. Imaging magnetic focusing of coherent electron waves. *Nat. Phys.* **2007**, *3*, 464−468.

(25) Bhandari, S.; Lee, G.-H.; Klales, A.; Watanabe, K.; Taniguchi, T.; Heller, E. J.; Kim, P.; Westervelt, R. M. Imaging Cyclotron Orbits of Electrons in Graphene. *Nano Lett.* **2016**, *16*, 1690−1694.

(26) Bhandari, S.; Lee, G.-H.; Watanabe, K.; Taniguchi, T.; Kim, P.; Westervelt, R. M. Imaging Electron Flow from Collimating Contacts in Graphene. *2D Mater.* **2018**, *5* (2), 021003.